http://dx.doi.org/10.5516/NET.08.2012.080

EFFECTIVE DOSE MEASUREMENT FOR CONE BEAM COMPUTED TOMOGRAPHY USING GLASS DOSIMETER

YOUNG MIN MOON[1,2], HYO-JIN KIM[1,2], DONG WON KWAK[2], YEONG-ROK KANG[1], MAN WOO LEE[1], TAE-IK RO[2], JEUNG KEE KIM[1], and DONG HYEOK JEONG[1*]
[1]Research Center, Dongnam Inst. of Radiological and Medical Sciences, Busan,619-953, Korea
[2]Department of physics, DongA University, Busan 604-714, Korea
[*]Corresponding author. E-mail : physics7@empas.com

Received November 08, 2012
Accepted for Publication September 25, 2013

During image-guided radiation therapy, the patient is exposed to unwanted radiation from imaging devices built into the medical LINAC. In the present study, the effective dose delivered to a patient from a cone beam computed tomography (CBCT) machine was measured. Absorbed doses in specific organs listed in ICRP Publication 103 were measured with glass dosimeters calibrated with kilovolt (kV) X-rays using a whole body physical phantom for typical radiotherapy sites, including the head and neck, chest, and pelvis. The effective dose per scan for the head and neck, chest, and pelvis were 3.37±0.29, 7.36±0.33, and 4.09±0.29 mSv, respectively. The results highlight the importance of the compensation of treatment dose by managing imaging dose.

KEYWORDS : Effective Dose, Cone Beam Computed Tomography, Image Guided Radiotherapy

1. INTRODUCTION

The purpose of image-guided radiation therapy (IGRT) [1] is to deliver precise radiation doses to target locations in a patient using three-dimensional images obtained from imaging devices attached to the medical LINAC. The adaptive radiotherapy technique [2], one of the new techniques in current radiotherapy, evolved from the IGRT modality via monitoring of treatment volumes of a patient using a high-performance imaging device such as a cone beam computed tomography (CBCT) machine. Kilovolt (kV) or megavolt (MV) based imaging devices [3] are currently used in IGRT. Recently, more attention has been paid to the additional imaging dose delivered to the patient from the imaging devices, which might increase a secondary cancer risk. Typically, the imaging dose has been significantly studied in diagnostic radiation use but there is a lack of experimental data on the imaging dose in CBCT. Goetti et al. [4] measured imaging dose using a thermoluminescence dosimeter (TLD) for two CBCTs in radiotherapy. However, the TLD has high uncertainty because of a high response to kV X-rays and directional dependency [5]. Hyer et al. used optical-fiber-based scintillation detectors [6], but an optical-fiber-based dosimetry device is not practical in a clinical setting because of its complex configuration and fragility [7]. As another approach, Hyer et al. studied the conversion of imaging dose using software operated by dose data for conventional CT scanners. As a result, large differences from the measured data [8] were observed because of the sensitivity of the organ doses to the scan protocol (scan geometry, kV, and mAs). In this study, effective doses from a CBCT machine for three typical radiotherapy sites were evaluated by measuring individual organ doses in an anthropomorphic physical phantom. Commercial glass dosimeters, which were specially designed for dosimetry in low-energy X-ray regions, were used in the measurements. One of the advantages of the glass dosimeter is the absence of directional dependency owing to its cylindrical symmetry [9]. The measured organ doses and effective doses are discussed in terms of patient safety in radiotherapy.

2. MATERIAL AND METHODS

2.1 CBCT System

The organ dose delivered from an X-ray volume imaging CBCT system (XVI™, Elekta, UK) built into a medical LINAC (Infinity™, Elekta, UK)(Fig. 1) was measured using a RANDO® phantom (The Phantom Laboratory, USA) and glass dosimeter. The Elekta Infinity system is a comprehensive treatment system that includes an IGRT feature. 3-D image guidance is designed to reduce position setup errors during treatment.

Table 1. Scanning Parameter

Scan Condition						
kVp	mA	Gantry Speed	Frames	Total mAs	Acquisition angle	Scan size (for head, chest and pelvis scans)
120	40	360 deg/min	660	1056	180°-180° cc	26.5×26.5 cm^2

Fig. 1. Elekta Infinity System Equipped with XVI CBCT System and RANDO Physical Phantom Placed on the Patient Bed

XVI is an electronic imaging device designed with a kV X-ray source and flat-panel detector mounted on the gantry for kV image acquisition. It provides more information to set up the patient position more accurately for treatment. The X-ray beam of the imaging system has the same isocenter as the MV treatment beam. In this study, the effective dose was evaluated using the scanning parameters listed in Table 1.

2.2 Physical Anthropomorphic Phantom

The RANDO® Woman phantom, which was used in this study, represents a 163 cm tall and 54 kg female without arms and legs as shown in Fig. 2. The phantom is constructed with the skeleton of a natural human, soft tissue and lung material. The human skeleton is cast inside soft tissue-simulating material; lungs are also molded to fit the contours of the natural rib cage. The phantom is sliced at an interval of 2.5 cm with holes in grid patterns, which are drilled into the sliced sections to enable the insertion of dosimeters.

2.3 The Beam Quality for kV X-ray from CBCT

In order to determine the X-ray beam quality, half-value layer (HVL) or effective energy was used as the beam quality index in the kV X-ray dosimetry protocol, where the effective energy is defined as the energy of a monoenergetic photon beam that yields the same HVL as a heterogeneous beam. In this study, the HVL of 7 mm Al was obtained from William et al. [10]. Then we determined the effective energy from the relationship, HVL=0.693/μ, where μ is the linear attenuation coefficient. The linear attenuation coefficients and HVLs of aluminum as a function of energy are listed in Table 2 [11].

Fig. 2. Frontal View of the RANDO® Female Phantom.

Table 2. Linear Attenuation Coefficients and HVLs of Aluminum According to the Effective Energies

Energy (keV)	Attenuation coefficient of aluminum (1/cm)	Half Value Layer (mm Al)
10	69.69	0.09944
15	21.15	0.3277
20	9.155	0.7570
30	3.009	2.303
40	1.520	4.561
50	0.9865	7.028
60	0.7457	9.290
80	0.5430	12.76
100	0.4591	15.10

The fitting curve of the effective energies for the HVLs of 4–12 mm Al is shown in Fig. 3.

The fitted equation for the effective energy according to the HVL of Al is as follows:

$$E_{eff} = 16.81 + 6.574 \times HVL - 0.4307 \times HVL^2 + \times 0.02385(HVL)^3, \quad (1)$$

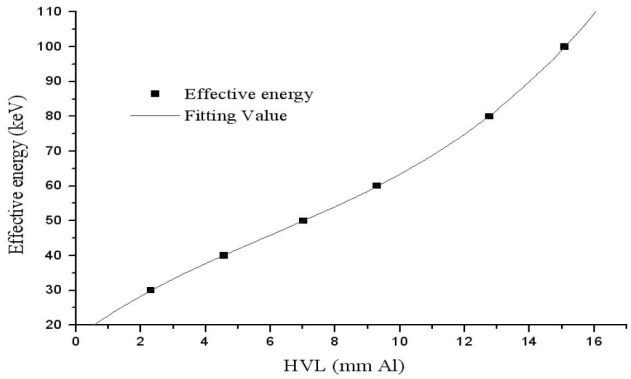

Fig. 3. Effective Energy for HVLs of 4-12 mm Al and Fitting Curve

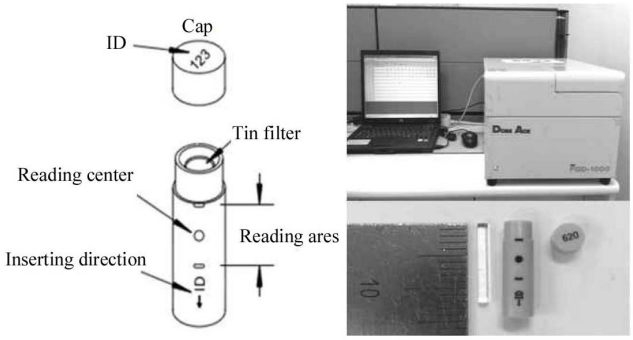

Fig. 4. Glass Dosimeter (GD352M) and Reader (FGD1000)

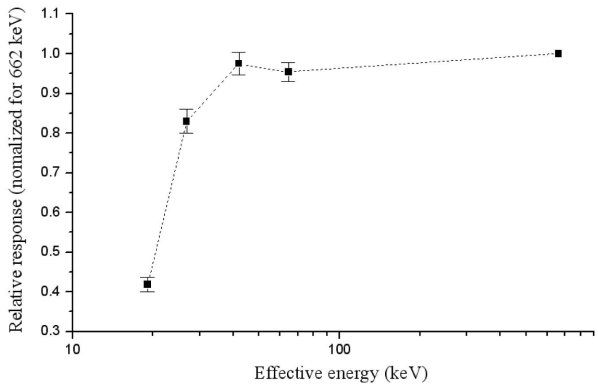

Fig. 5. Relative Response for Effective Energy

where E_{eff} is effective energy and *HVL* is half-value layer. The effective energy for XVI was 49.9 keV, which was cal-culated using equation (1).

2.4 Dosimetry System

A glass dosimeter is an accumulation type solid state dosimeter, which is based on the radiophotoluminescent phenomenon of silver activated phosphate glass. The glass dosimetry system is composed of rod-shaped silver activated phosphate glass, a plastic capsule, and an automatic reader unit. The weight compositions of the glass dosimeter are as follows: P (31.55%), O (51.16%), Al (6.12%), Na (11.0%) and Ag (0.17%). The effective atomic number and density are 12.039 and 2.61 g/cm^2 respectively. Measurable doses range from 10 mGy to 10 Gy in standard mode and from 1 to 500 Gy in high dose mode. In this study, a GD352M glass dosimeter (Asahi Techno Glass, Japan) designed for low energy photon beams was used [12]. The GD352M is shown in Fig. 4. In the figure a tin filter compensates for the high response in low energy photons. Detailed information for the glass dosimeter is described in ref. [13].

In air kerma based dosimetry, the absorbed dose in air can be expressed by

$$D_{air} = K_{air}(1 - g), \quad (2)$$

where D_{air} and K_{air} are absorbed dose and kerma in air, respectively, and g is the bremsstrahlung fraction. In kilovoltage X-rays, g is generally ignored; therefore, the air kerma becomes approximately the same as the absorbed dose in air [14]. In this study, air kerma based dosimetry was used. The reader was calibrated by air kerma for gamma rays from a Cs-137 source. The variation of response in different beam quality from Cs-137 gamma rays was carefully considered in reading the dosimeter. In order to correct the beam quality, five glass dosimeters were exposed to standard irradiation with M30, M60, M100, M150 kV X-rays, and Cs-137 gamma rays in the standard dosimetry laboratory of KAERI (Korea Atomic Energy Research Institute).

The beam quality factor *k* was inferred from the standard irradiations. The *k* as a function of beam quality (Q) was calculated by

$$\mathrm{k(Q)} = \frac{Respose\ per\ unit\ kerma\ for\ a\ reference\ quality}{Response\ per\ unit\ Kerma\ for\ a\ quality, Q}. \quad (3)$$

Therefore the absorbed dose in air for kV X-rays is calculated by

$$D_{air,Q} = D_{air,Qo} \times k(Q), \quad (4)$$

where $D_{air,g}$ is the absorbed dose in air for a beam quality Q, and $D_{air,Qo}$is the absorbed dose in air by reference beam quality Q_0.

Effective energy was directly employed as the beam quality parameter ($Q = E_{eff}$) and *k* (=*1.040*) was determined for E_{eff} = 49.9 keV by a linear interpolation using relative response data. The relative response normalized by Cs-137 gamma rays is shown in Fig. 5.

2.5 Measurement of Organ Doses

The phantom was positioned similarly to a real patient being treated for a particular anatomical region to achieve clinically suitable dose values. For head and neck scans,

the phantom was aligned with the center of the philtrum at isocenter of the treatment beam. The irradiated region during CBCT included part of the esophagus, thyroid, salivary glands, oral mucosa, extrathoracic region, and brain. For chest scans, the beam isocenter was placed in the center of the body at an axial plane near the center of the lungs. The region of interest in the chest scan covered the lungs, part of the esophagus, breast, liver, thymus, heart, spleen, adrenals, pancreas, gall bladder, kidneys, part of the small intestine, and stomach. For pelvis scans, the center of the sacrum was placed at the beam isocenter. The irradiated region in the pelvis scan consisted of the colon, ovaries, small intestine, cervix, and bladder. To ensure reproducibility, cross hairs at the anterior and the lateral side were marked and always aligned with the cross line of the laser pointer.

To measure organ doses, the glass dosimeters were inserted in the holes of the phantom which are positioned in the volume of the organs listed in the ICRP (International Commission on Radiation Protection Publication)-103 recommendations [15]. Table 3 shows all of the organs investigated and the number of measurement locations used to evaluate the organ dose.

The average dose to skin was evaluated by placing 6 dosimeters at the center of the anterior and left lateral marked cross lines for head and neck, chest, and pelvis scan.

Table 3. List of Organs and Tissues Investigated in the Study and the Number of Measurement Points

Organ	Phantom slice number	Measurement Points
Brain	3	2
Esophagus	6, 11	2
Salivary glands	6	2
Thyroid	9	2
Lungs	13, 17	4
Breast	17	2
Stomach	21	1
Liver	21	1
Colon	26	2
Gonads (Ovaries)	28	2
Bladder	32	1
Bone marrow	6, 13, 18, 21, 25, 28, 32	13
Bone surface	6, 13, 18, 21, 25, 28, 32	13
Skin	6, 18, 30	6
Reminder Organ:		
Oral mucosa	7	1
Extrathoracic region	6, 7, 9	4
Thymus	14	1
Heart	18	1
Spleen	20	1
Adrenals	21	2
Pancreas	21	1
Gall bladder	22	1
Kidneys	22	2
Small intestine	24,25	2
Cervix	33	1

For small organs, absorbed doses measured near the center of the organ were adopted as the organ dose. For larger organs, dosimeters were placed within the volume of the organ which was evenly subdivided. A mass energy absorption coefficient obtained from the ICRU (International Commission on Radiological Unit and measurement) Report 44 [16] was employed. The organ absorbed dose was calculated using the following equation:

$$D_{organ} = D_{air} \times (\frac{\mu_{en}}{\rho})_{air}^{organ} \times k(Q), \quad (5)$$

where D_{organ} is dose in the organ, D_{air} is dose in air, and $(\frac{\mu_{en}}{\rho})_{air}^{organ}$ is the ratio of mass energy absorption coefficients in organ to air.

2.6 Calculation of Effective Doses

After the calculation of the organ absorbed doses, the effective dose was evaluated as follows:

$$H_E = \sum_T (D_{RT} \times W_R \times W_T), \quad (6)$$

where H_g is the effective dose, D_{RT} is the absorbed dose delivered by radiation type R averaged over organ T, W_R is the radiation-weighting factor, and W_T is the tissue-weighting factor. In our case, the organ dose is simply the equivalent dose because the radiation weighting factor for X-rays from CBCT is 1.0. In this study, the effective dose was derived using only the female physical phantom, but according to ICRP-103 recommendations the effective dose is defined for the average of male and female. It must be noted that the effective dose derived in this study is an approximation of actual effective dose. Takahiko Aoyama et al. [19] reported that female and male-specific effective doses were not significantly different.

The doses to lymphatic nodes and muscle as remainder organs listed in ICRP-103 were not measured as in other previous studies [17] [20]. The fact that these tissues are evenly distributed across the human body makes it technically difficult to measure average dose to the tissues. Nevertheless, these two reminder tissues do not contribute significantly to the overall effective dose because of their small tissue weight factors. In conclusion, the average dose to the other 11 remainder organs was used for the effective dose evaluation.

3. RESULT AND DISCUSSION

The organ and effective doses measured using the standard CBCT mode for the three different treatment sites (head and neck, chest, and pelvis) are shown in Table 4.

3.1 Head and Neck Scan

The thyroid received a maximum dose of 26.6 mGy, which was much higher than those of other in-field organs; the esophagus, salivary glands, oral mucosa, extrathoracic region, and brain received 12.0, 20.1, 18.4, 23.0, and 17.2 mGy, respectively. The points of measurement for the thyroid were adjacent to the trachea. The relatively higher dose in the thyroid is attributed to the reduced X-ray attenuation through the air cavity and the smaller diameter of the neck. For organs that were not covered by the primary beam, the measured doses were much smaller than those of the in-field organs. The effective dose in this scan was 3.67 mSv. The relatively higher doses of the thyroid, salivary glands, and esophagus were major contributors to the effective dose.

3.2 Chest Scan

The glass dosimeter data showed that the organ dose within the irradiated site varied from 7.15 to 16.8 mGy. A maximum dose of 16.8 mGy was found in the thymus, and the point of measurement was close to the junction of the aorta and heart. The presence of the lung, neck, and thin skin layer around the thymus increased the backscattering radiation dose to the tissue. For the points covered by the primary beam, the glass dosimeter data showed a mean dose of 14.1 mGy. For the chest scan, the doses to organs adjacent to the in-field organs ranged from 0.105 to 1.01 mGy. The effective dose from the single CBCT scan of the chest was estimated to be 7.36 mSv.

3.3 Pelvis Scan

The bladder received a maximum dose of 13.0 mGy. A dose of 9.89 mGy was observed in the small intestine. Doses ranging from 0.0769 to 1.85 mGy were found for organs that were not irradiated directly by the primary beam. The average organ dose for the stomach, liver, adrenals, pancreas, gall bladder, and kidneys adjacent to the pelvis were relatively higher, up to 1.31 mGy, because the high density of the pelvis resulted in a high probability for scattering. The effective dose for the pelvis scan was 4.09 mSv.

3.4 Discussion

Calibration for the energy dependence of the detector is required to obtain accurate measurement values. In this study, the GD352M, which was corrected for the high response in kV energies of X-rays, was calibrated again for more accurate measurement of the imaging dose from the XVI system. As a result, the beam quality coefficient was obtained and the corrected organ dose was 4.0% higher than the uncorrected organ dose.

It is important to differentiate the data in this study from that in other studies. For the XVI system, a small number of organ dose studies have been reported in the literature. Islam et al. measured doses using an ion chamber with MOSFET detectors and cylindrical water phantoms [21]. The doses were 1.8 to 2.3 cGy for 120 kV in a 30-cm diameter body phantom and 2.6 to 3.4 cGy for 120 kV in

Table 4. Organ Dose and Effective Dose for Head and Neck, Chest, and Pelvis Scans

Organ	Absorbed dose per scan (mGy)		
	Head and neck scan	Chest scan	Pelvis scan
Brain	17.2±1.3	0.196±0.027	0.0769±0.0437
Esophagus	12.0±0.4	7.15±0.54	0.202±0.048
Salivary glands	20.1±0.6	0.479±0.021	0.109±0.003
Thyroid	26.6±2.0	1.01±0.06	0.122±0.042
Lungs	1.58±0.11	14.5±1.1	0.244±0.066
Breast	0.337±0.024	9.16±0.59	0.316±0.043
Stomach	0.179±0.009	14.7±0.6	1.04±0.06
Liver	0.201±0.009	15.8±0.8	1.02±0.06
Colon	0.0984±0.0238	0.872±0.087	12.5±0.5
Gonads (Ovaries)	0.0517±0.0116	0.190±0.022	11.5±0.4
Bladder	0.0445±0.0111	0.153±0.022	13.0±0.5
Bone marrow	3.95±0.15	3.64±0.12	5.64±0.18
Bone surface	21.2±0.7	19.5±0.6	30.3±1.0
Skin	6.46±1.05	5.52±0.80	4.57±0.75
Reminder Organ:			
Oral mucosa	18.4±0.6	0.741±0.025	0.110±0.003
Extrathoracic region	23.0±1.0	0.915±0.044	0.113±0.003
Thymus	1.61±0.05	16.8±0.5	0.156±0.005
Heart	0.384±0.013	16.6±0.5	0.348±0.011
Spleen	0.232±0.007	16.0±0.5	0.639±0.021
Adrenals	0.170±0.005	14.5±0.4	1.10±0.03
Pancreas	0.166±0.005	15.7±0.5	1.12±0.03
Gall bladder	0.150±0.005	14.6±0.4	1.85±0.06
Kidneies	0.141±0.004	14.2±0.4	1.78±0.08
Small intestine	0.0917±0.0031	3.32±0.11	9.89±0.33
Cervix	0.0284±0.0011	0.105±0.007	12.6±0.4
Effective Dose	3.67±0.29 mSv	7.36±0.33 mSv	4.09±0.29 mSv

a head phantom. The doses depend on the size of the field of view, measurement depth, and the number of projections from the CBCT. Sykes et al. reported surface doses from 2.6 to 3.1 cGy for a setting of 130 kV, 40 mA, 14 ms, and 612 projection images in a RANDO® head phantom [22]. However, since these studies do not report organ-specific doses, it is not useful to compare their results with the organ doses in our study. Daniel E. Hyer et al. used optical-fiber-based scintillation detectors to measure effective dose for XVI and OBI cone-beam CT systems measurement [23]. For the head and neck, chest, and pelvis scan, the effective doses were 0.04, 7.15, and 3.73 mSv, respectively. The effective dose for the chest scan completely agrees with the value evaluated in this study. For the head and neck and the pelvis scan, the dose difference might be attributed to a considerable deviation in a setting for the CBCT scan.

Our study shows that the use of CBCT during treatment will deliver a considerable imaging dose (12.0–26.6 mGy

for head and neck scan, 9.16–16.8 mGy for chest scan, and 9.89–13.0 mGy for pelvis scan) to organs positioned in the primary imaging field. Notification about the imaging dose from the use of CBCT is important when used for daily position verification. Also it can be reduced through adjusting the scan parameters and the number of projections from CBCT.

4. CONCLUSIONS

The effective dose to patients from the X-ray volumetric imager attached to a medical LINAC was evaluated. Organ dose was measured using glass dosimeters, which were implanted at various organ positions within a RANDO® Woman phantom. The effective dose was evaluated according to the ICRP 103 recommendation. In the CBCT examination of the head and neck, chest, and pelvis, the organ doses from the primary beam were 12.0–26.6 mGy, 9.16–16.8 mGy, and 9.89–13.0 mGy, respectively, and the effective doses were 3.67 mSv, 7.36 mSv, and 4.09 mSv, respectively.

Generally, radiation therapy is performed with the fractions from 10 to 30 [24]. If the prescribed dose (PD) is 60 Gy and one CBCT scan is carried out for one treatment cycle, the imaging dose for the thyroid from the maximum dose in a head and neck scan during a 30-fraction treatment is 1.33% of PD at 79.8 cGy. In particular, the imaging doses for the thymus in a chest scan and the bladder in a pelvis scan are 0.84% of PD at 50.4 cGy and 0.65% of PD at 39.0 cGy, respectively.

The additional effective dose during the 30-fraction treatment ranged from 110 mSv (head and neck scan) to 220 mSv (chest scan). According to ICRP 103, the probability of fatal cancer risk from a single radiographic exposure is 5.5×10^{-5} per mSv. The effective dose from 110 to 220 mSv could induce an additional secondary cancer risk of about 0.6 to 1.2%. These data are expected to be useful in determining the number of CBCT scans performed in radiotherapy.

In order to clinically use the data, the effective dose should be evaluated for various scan conditions and scan sites. Further studies are required for the various scanning conditions of CBCT and different IGRT LINACS.

ACKNOWLEDGEMENT

This research was supported by the National R&D Program through the Dong-nam Institute of Radiological & Medical Sciences (DIRAMS) funded by the Ministry of Education, Science and Technology (50497-2012)

REFERENCES

[1] Létourneau D, Wong JW, Oldham M, et al., "Cone beam-CT guided radiation therapy", Radiat Oncol, vol. 75, pp. 279-286 (2005).
[2] McBain CA, Henry AM, Sykes J, et al., "X-ray volumetric imaging in image-guided radiotherapy", Radiat Oncolm vol.64, pp. 625-634 (2006).
[3] Amies C, Bani-Hashemi A, Celi JC, et al.,"A multiplatform approach to image guided radiation therapy (IGRT)", Med Dosim,vol. 31, pp. 12–19 (2006).
[4] Robert Goetti, Sebastian Leschka, Markus Boschung, et al., "Radiation doses from phantom measurements at high-pich dual-source computed tomography coronary angiography". Eur J Radiol, vol. 81,pp. 773–779 (2012).
[5] C R Edwards,PhD Mipem and P J Mountford, et al.,"The low energy X-ray response of the LiF:Mg:Cu:P thermoluminescent dosemeter: a comparison with LiF:Mg:Ti",British Journal of Radiology, vol. 78, pp. 543-547 (2005).
[6] Hyer DE, Fisher RF and Hintenlang DE,"Characterization of a water-equivalent fiber-optic coupled dosimeter for use in diagnostic radiology", Med Phys. vol. 36, pp.1711-1716 (2009).
[7] Marckmann CJ, Aznar MC, Andersen CE and Bøtter-Jensen L,"Influence of the stem effect on radioluminescence signals from optical fibre Al2O3:C dosemeters", Radiat Prot Dosimetry,vol. 119, pp. 363–67 (2006).
[8] Daniel E and Hyer, et al., "Estimation of organ doses from kilovoltage cone-beam CT imaging used during radiotherapy patient position verifivation", Med. Phys, vol. 37, pp. 4020-4026 (2010).
[9] Shih-Ming Hsu, Hsi-WenYang and Tien-ChiYeh, et al., "Synthesis and physical characteristics of radiophotoluminescent glass dosimeters",Radiation Measurements, vol. 42, pp. 621 – 624 (2007).
[10] William Y. Song,a, Srijit Kamath and Shuichi Ozawa, et al., "A dose comparison study between XVI® and OBI® CBCT systems",Med. Phys, vol. 35, pp. 480-486 (2008)
[11] Khan FM, The physics of radiation therapy, 3rd ed., p.647, Lippincott Williams & Wilkins, Philadelphia USA (2003).
[12] ASAHI Glass Cor, FGD-1000 introduction manual, p. 16 , ASAHI Glass Cor, Tokyo (2004).
[13] ASAHI Glass Cor, RPL Glass Dosimeter / Small Element System, ASAHI Glass Cor, Tokyo (2007).
[14] Ervin B and Podgorsak, Review of Radiation Oncology Physics: A Handbook for Teachers and Students, p. 49, International Atomic Energy Agency, Vienna (2003).
[15] ICRP Publication 103, "The 2007 Recommendations of the International Commission on Radiological Protection", The International Commission on Radiological Protection (2007).
[16] ICRU, "Tissue Substitutes in Radiation Dosimetry and Measurement", Report 44, The International Commission on Radiation Units and Measurements (1989).
[17] Kawaura C, Aoyama T, Koyama S, Achiwa M and Mori M, "Organ and effective dose evaluation in diagnostic radiology based on in-phantom dose measurements with novel photodiode-dosemeters", Radiat Prot Dosimetry. vol. 118, pp. 421-430 (2006).
[18] ICRP Publication 70, "Basic anatomical and physiological data for use in radiological", The International Commission on Radiological Protection (1995).
[19] Takahiko Aoyama, Shuji Koyama and Chiyo Kawaura, "Organ dose measurement in x-ray CT and other diagnostic radiology by using novel photodiode dosimeters installed in an anthropomorphic phantom", 11th International Congress of the International Radiation Protection Association (IRPA

11), Madrid, Spain, May. 23-28(2004).
[20] Lee C, Lodwick D, Hurtado J, Pafundi D and Bolch WE, "Development of a series of hybrid computational phantoms and their applications to assessment of photon and electron specific absorbed fractions", 2008 Annual Meeting of the European Association of Nuclear Medicine, Munich, Germany,Feb. 13-15 (2008).
[21] Islam MK, Purdie TG and Norrlinger BD, et al., "Patient dose from kilovoltage cone beam computed tomography imaging in radiation therapy", Med Phys, vol. 33, pp. 1573–1582 (2006).
[22] Sykes JR, Amer Ali and Czajka J, et al., "A feasibility study for image guided radiotherapy using low dose, high speed, cone beam X-ray volumetric imaging", Radiat Oncol,vol. 77, pp. 45–52 (2005).
[23] Daniel E. Hyer, Christopher F. Serago, Siyong Kim, Jonathan G. Li and David E. Hintenlang, "An organ and effective dose study of XVI and OBI cone-beam CT systems", Med Phys, vol. 11, pp. 181-197 (2010).
[24] Byung Chul Cho, et al, "Guideline for Imaging Dose on Image-Guided Radiation Therapy", PROGRESS in MEDICAL PHYSICS, vol. 24, pp. 1-24 (2013).